

Developments in the Calculation of Fission Potential-Energy Surfaces

Peter MÖLLER^{1,*}, David G. MADLAND¹, Arnold J. SIERK¹, and Akira IWAMOTO²

¹Theoretical Division, Los Alamos National Laboratory, Los Alamos, New Mexico 87545, USA

²Department of Materials Science, Japan Atomic Energy Research Institute, Tokai-mura, Naka-gun, Ibaraki, 319-1195 Japan

We present calculations based on a realistic theoretical model of the multi-dimensional potential-energy surface of a fissioning nucleus. This surface guides the nuclear shape evolution from the ground state, over inner and outer saddle points, to the final configurations of separated fission fragments. Until recently, no calculation has properly explored a shape parameterization of sufficient dimensionality to permit the corresponding potential-energy surface to exhibit the multiple minima, valleys, saddle points and ridges that correspond to characteristic observables of the fission process. Here we calculate and analyze five-dimensional potential-energy landscapes based on grids of several million deformation points. We find that observed fission features such as different energy thresholds for symmetric and asymmetric fission and fission-fragment mass and kinetic-energy distributions are very closely related to properties of the valleys and mountain passes present in the calculated five-dimensional energy landscapes. We have also determined fission-barrier heights for 31 nuclei throughout the periodic system.

KEYWORDS: *nuclear fission, fission barrier, multi-mode fission*

I. Introduction

When a heavy nucleus divides into two fragments in nuclear fission, two key aspects of the process have challenged researchers since the discovery of fission more than 60 years ago. First, what is the threshold energy for the reaction and, second, what are the shapes involved in the transition from a single nuclear system to two separated daughter fragment nuclei? These two questions are intimately connected. The energy of a nucleus as a function of shape defines a landscape in a multi-dimensional deformation space. It is the energy of the lowest mountain pass, or saddle point, in this landscape, connecting the nuclear ground state with the region corresponding to separated fragments that represents the threshold energy of the fission process.

After the discovery of fission in 1938 by Hahn and Strassmann¹⁾ the phenomenon was almost immediately explained by Meitner and Frisch²⁾ and by Bohr and Wheeler³⁾ in terms of a model involving a charged liquid drop with a surface tension. When the atomic number increases, the drop becomes increasingly unstable with respect to deformation and at proton number $Z \approx 100$ stability is completely lost. For slightly lower- Z actinide nuclei the fission *barrier* between the ground-state shape and the separated-fragment configuration is sufficiently small that spontaneous fission, due to quantum-mechanical penetration of the fission barrier, occurs with measurable probability. Fission may also be induced by exciting the nucleus to energies above the barrier energy. In some cases, such as $n+^{235}\text{U}$, thermal neutron capture yields sufficient energy to excite the nucleus above the barrier.

In a pioneering use of the first electronic digital computer ENIAC, Frankel and Metropolis⁴⁾ in 1947 explored some key aspects of the liquid-drop-model potential-energy landscape. In particular, they determined the shapes of nuclei at the saddle point threshold energies in the macroscopic model they investigated. However, no macroscopic model such as the

liquid-drop model of nuclear fission is able to explain certain features of fission-fragment mass and kinetic-energy distributions. For example:

1. Nuclei near ^{228}Ra exhibit two fission modes. We show in **Fig. 1** an example of the extensive data obtained in Reference.⁵⁾ In one mode, with the lower threshold energy, the fragment mass distribution is asymmetric and the fragment total kinetic energy is about 10 MeV higher than in the other, symmetric mode. The kinetic energies indicate that the scission configuration is more compact for the asymmetric mode than for the symmetric mode. From the totality of the data Ref.⁵⁾ concludes: “Thus it seems that after the gross determination of the symmetric or asymmetric character of fission made already at the barrier, the two components follow a different path with no or little overlap in the development from the barrier to the scission configuration.”

Here in Japan it has been determined that many nuclei in the light actinide region exhibit similar fission properties.⁶⁻⁸⁾

2. Most actinide nuclei near the line of β stability undergo mass-asymmetric fission. The heavy-fragment mass is close to 140 from Th to Fm, with the remainder of the mass in the light fission fragment.
3. Near the upper end of the actinide region fission properties change suddenly and may exhibit a different type of bimodal character in the same nucleus. For example, the fragment mass distribution changes suddenly from mass-asymmetric for ^{256}Fm to symmetric for ^{258}Fm and there is a correlated *increase* in the total fragment kinetic energy (TKE) by 35 MeV. But ^{258}Fm also exhibits the asymmetric mode with the lower TKE.

In the 1960s an improved model for the nuclear potential energy as a function of shape emerged. In this *macroscopic-microscopic* model,^{9,10)} the potential energy is the sum of

* Corresponding author, Tel. +1-505-665-2210, Fax. +1-505-667-1931, E-mail: moller@moller.lanl.gov

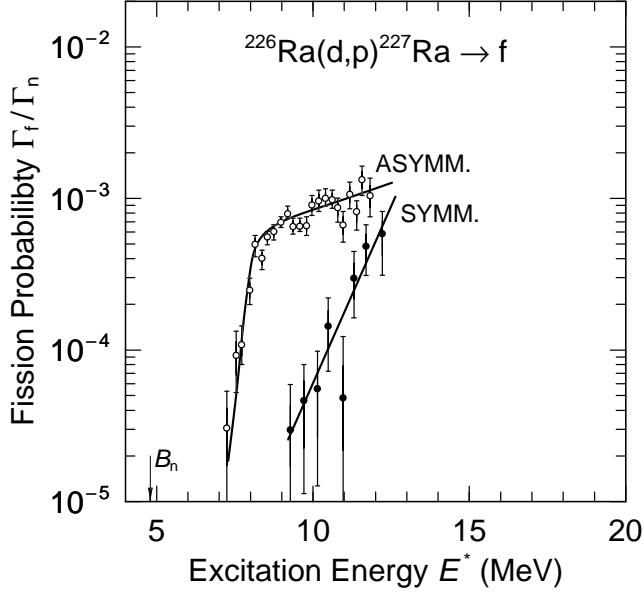


Fig. 1 Fission probability data show different thresholds for mass-asymmetric and mass-symmetric fission for ^{227}Ra . The figure is based on a figure in Ref.⁵⁾

shape-dependent liquid-drop and microscopic terms. Over the past 30 years this model has provided considerable insight into nuclear structure. For example nuclear masses are calculated for nuclei throughout the periodic system to an average accuracy of about 0.7 MeV. Improved descriptions of the fission barrier, for example fission-isomeric states and mass-asymmetric fission saddle points were obtained in this model.

However, since the spurt of insights in the early 1970s no major improvement in the description of the fission potential-energy landscape has been obtained. Many calculations based on 1000 or so grid points have been presented. But, to properly describe the evolution of a single nuclear shape into two fragments* of different mass and deformation, for example one spherical ^{132}Sn -like fragment and one deformed fragment with mass number A near 100, at least five independent shape parameters are required. We have here constructed, calculated, and investigated such a five-dimensional space with 2 610 885 grid points. Specifically, the five shape coordinates are: (1) charge quadrupole moment, (2) neck diameter, (3) left nascent-fragment deformation, (4) right nascent-fragment deformation, and (5) mass asymmetry.

II. Model

Our potential-energy model is the macroscopic-microscopic finite-range liquid-drop model as defined in Ref.¹¹⁾ with shape-dependent Wigner and A^0 terms as defined in Ref.¹²⁾ In fission-barrier calculations it is essential to formulate the model so that the energy obtained for the configuration of two touching spherical nuclei is the same

*At the present time we do not consider parameterizations that allow the study of ternary fission. However, at low excitation energy only approximately one in five hundred fissions are ternary in the actinide region.

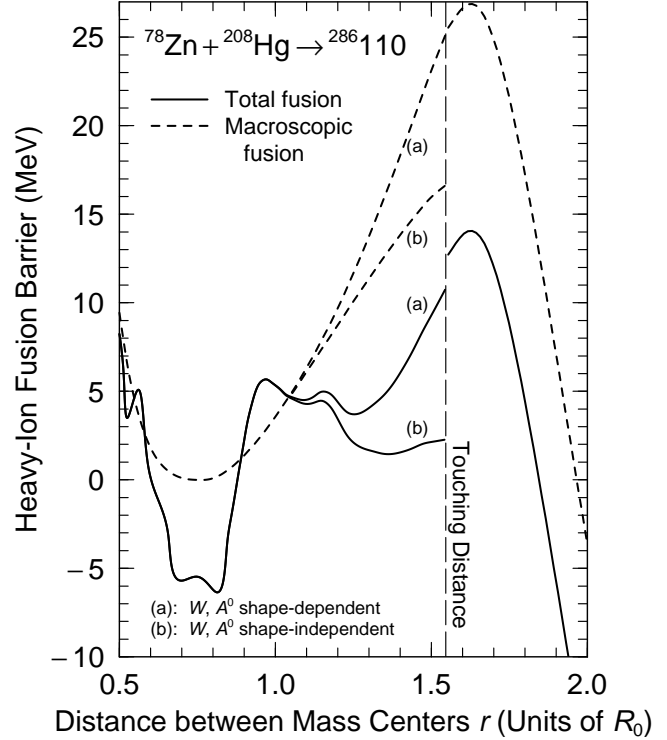


Fig. 2 Calculated macroscopic and total potential energies for shape sequences leading to the touching configuration, at the long-dashed line, of spherical ^{78}Zn and ^{208}Hg

To the left the calculations trace the energy for a *single, joined* shape configuration from oblate shapes through the spherical shape at $r = 0.75$ to the touching configuration at $r = 1.52$; to the right the calculations trace the energy for separated nuclei to the touching point. To obtain continuity of the energy at touching, a crucial, necessary feature in realistic models, it is essential that various model terms depend appropriately on nuclear shape, as is the case for the curves (a). The slight remaining discontinuity in the total fusion energy curve arises because the Fermi surfaces of the nuclei readjust at touching, and because pairing and spin-orbit terms also change discontinuously there.

whether the energy is calculated as that of a very deformed compound system or as that of two separate nuclei with appropriate Coulomb and nuclear interaction energies. By introducing shape dependencies for the Wigner and A^0 terms in the macroscopic part of the model and implementing other features in the microscopic part, we have assured that the model has the required properties. These issues are discussed in further detail in Refs.^{12,13)} It is not possible to formulate the droplet model satisfactorily in the limit of the touching configuration; for this reason we use the FRLDM version in our calculations instead of the FRDM. In **Fig. 2** we show that when appropriate shape dependencies are included for the Wigner and A^0 terms then we obtain approximate continuity at touching: almost the same energy is obtained for a very deformed shape with zero neck radius as for

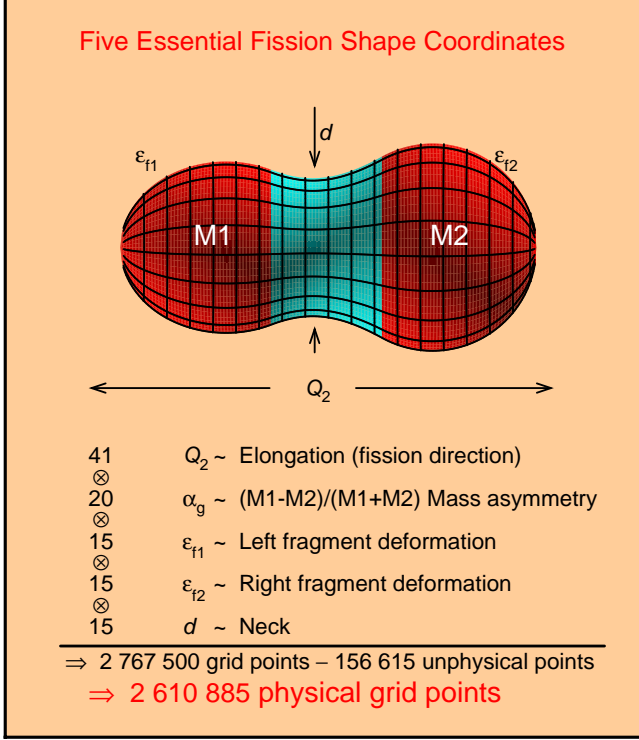


Fig. 3 Five-dimensional shape parameterization used in the present potential-energy calculation

Different shades of gray indicate the three different quadratic surfaces defined in the 3QS. The first derivative is continuous where the surfaces meet. Note that we give the charge quadrupole moment Q_2 in terms of ^{240}Pu with the same shape as the nucleus considered, so that the nuclear size effect is eliminated. The end body masses, or equivalently volumes, M_1 and M_2 , refer to the left and right nascent fragments were they completed to closed shapes. For the nascent spheroidal fragments we characterize the deformations by Nilsson’s quadrupole ϵ parameter.

(the identical) configuration of separate, but just touching, spherical daughter fragments.

III. Shape Parameterization

Because fragment shell effects strongly influence the structure of the fission potential-energy surface long before scission, often in the outer saddle region, it is crucial to include in calculations the nascent-fragment deformations as two independent shape degrees of freedom. In addition, elongation, neck diameter, and mass-asymmetry shape degrees of freedom are required, at a minimum, to adequately describe the complete fission potential-energy surface. For nascent-fragment deformations we choose spheroidal deformations characterized by Nilsson’s quadrupole ϵ parameter. This single fragment-deformation parameter is sufficient because higher-multipole shape-degrees of freedom are usually of lesser importance in the fission-fragment mass region below the rare earths.

The three-quadratic-surface parameterization (3QS) is ideally suited for the above description.¹⁴⁾ In the 3QS the shape of the nuclear surface is specified in terms of three smoothly joined portions of quadratic surfaces of revolution. Using this parameterization we here construct, calculate, and investigate complete five-dimensional spaces with 2 610 885 grid points as illustrated in **Fig. 3**.

A common notation used to characterize the fragment mass asymmetry of a fission event is M_H/M_L where M_H and M_L are the masses of the heavy and light fission fragments respectively. For the purpose of grid generation for the potential-energy calculation it is convenient to relate a mass-asymmetry shape degree of freedom for the pre-scission nucleus to the final fission-fragment mass asymmetry in some fashion, although the final mass division, strictly speaking, cannot be determined from the static shapes occurring before scission. However, the exact nature of our definition of mass asymmetry for a single shape has little effect on the calculated saddle-point energies and shapes because our five-dimensional grid covers all of the physically relevant space available to the 3QS parameterization, regardless of how we choose to define a “mass-asymmetry” coordinate. In order to obtain a definition of mass asymmetry that is meaningful close to scission, and equations that are reasonably simple to work with for the purpose of grid-point generation, we define an auxiliary grid mass-asymmetry parameter α_g

$$\alpha_g = \frac{M_1 - M_2}{M_1 + M_2} \quad (1)$$

where M_1 and M_2 are the volumes inside the end-body quadratic surfaces, were they completed to form closed-surface spheroids. Thus

$$\alpha_g = \frac{a_1^2 c_1 - a_2^2 c_2}{a_1^2 c_1 + a_2^2 c_2} \quad (2)$$

where a denotes the transverse semi-axis and c the semi-symmetry axis of the left (1) and right (2) quadratic surfaces of revolution. With this definition we select 20 coordinate values corresponding to

$$\alpha_g = -0.02 \dots (0.02) \dots 0.36 \quad (3)$$

We have closely spaced the asymmetry coordinate so that we will be able to spot favorable saddle-point shapes that may not appear in a more sparsely spaced grid. For ^{240}Pu the values 0.00, 0.02, and 0.36 of the mass-asymmetry coordinate α_g correspond to the mass divisions 120/120, 122.4/117.6, and 163.2/76.8, respectively.

Because of the intuitive appeal of the notation M_H/M_L we use it below to characterize the “asymmetry” of a single shape. We then connect M_H and M_L to α_g through

$$M_H = A \frac{1 + \alpha_g}{2} \quad \text{and} \quad M_L = A \frac{1 - \alpha_g}{2} \quad (4)$$

for a nucleus with A nucleons. For shapes with a well-developed neck the ratio obtained with this definition can be expected to be close to the final fragment mass-asymmetry ratio. We cannot conveniently use M_1 and M_2 to designate the

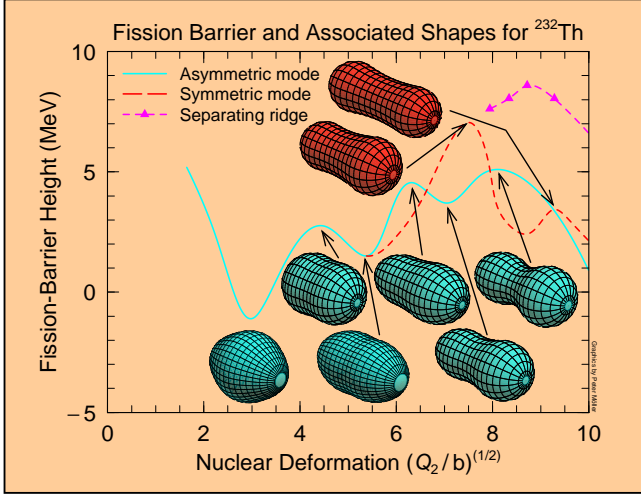


Fig. 4 Fission barriers for symmetric and asymmetric fission modes for ^{232}Th

The ridge between the two valleys is also shown. The shapes shown correspond to saddle points and minima along the two fission barriers. The entry saddle point to the symmetric valley is 2.17 MeV higher than the entry saddle point to the asymmetric valley. The highest point on the separating ridge is 1.56 MeV higher than the symmetric saddle. All energies are given relative to the spherical macroscopic energy.

final fragment mass asymmetries because they do not exactly sum up to the total nuclear volume or mass. Equation (4) simply represents a scaling of M_1 and M_2 so that their sum after scaling adds up to the total mass number A .

We have performed several multi-million grid-point calculations for different regions of nuclei, down to ^{70}Se . For fission-fusion potential-energy surfaces in the superheavy-element region we have extended the range of the mass-asymmetry coordinate to $\alpha_g = 0.66$. The corresponding deformation space consisted of 3 637 478 deformation grid points when 33 different elongations (Q_2) were considered.

IV. Analysis of Five-Dimensional Spaces

It is a common misconception that the structure of a multi-dimensional potential-energy function can be determined by calculating and displaying the function versus two shape variables, for example, β_2 and β_3 where the function has been “minimized” with respect to additional multipoles such as β_4 , β_5 , β_6 and β_7 . Such approaches are not even approximately correct. No such “local” strategy will correctly identify saddle points in multidimensional spaces as is extensively discussed in Refs.^{15–17)}

It is *also* a common misconception that *constrained* self-consistent calculations, for example HF or HFB calculations with Skyrme or Gogny forces^{21–23)} automatically take into account all non-constrained variables. For the application to saddle-point determination this is incorrect. A self-consistent calculation constrained in one variable, for example Q_2 , would have difficulties similar to those discussed above.

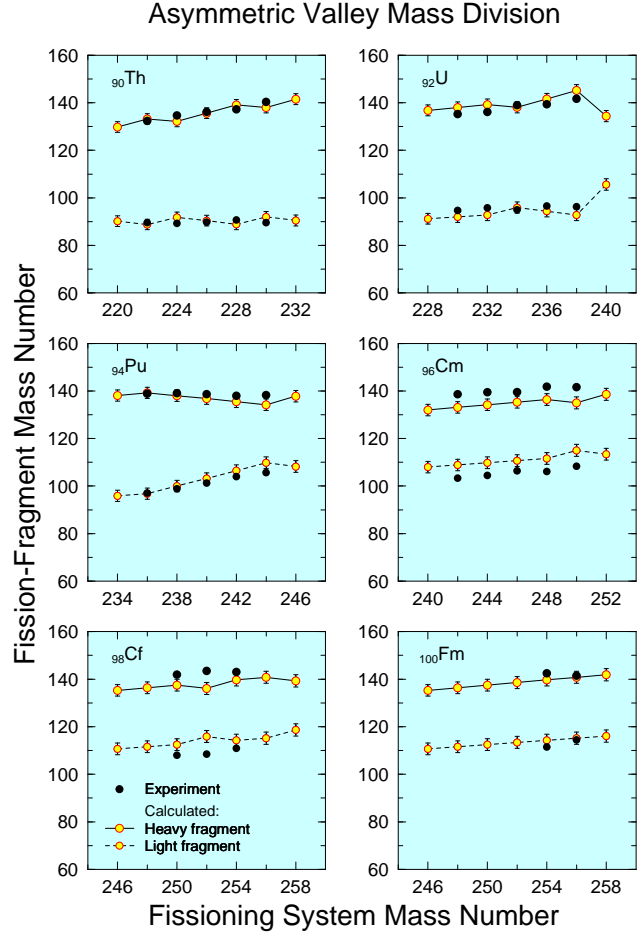


Fig. 5 Calculated and measured^{18–20)} average mass division in asymmetric fission for sequences of even isotopes of Th, U, Pu, Cm, Cf, and Fm

The error bars on the calculated points correspond to the spacing of mass asymmetry values on the multidimensional shape-coordinate grid. The data is for spontaneous fission when it is available, otherwise data for low-energy induced fission is used. The results reproduce the experimental observation of a heavy fragment at mass number $A \sim 140$ and a light fragment with mass corresponding to the remainder of the original nucleus. However, deviations from this rule of thumb are also reproduced by the calculations.

In addition, it is of interest to note that in calculations where the potential energy is displayed as contour diagrams versus two shape variables and in which the energy is minimized with respect to additional multipoles, only relatively few points are required to perform a minimization with respect to, say, 3 additional multipoles, about 30 or so. If the two-dimensional contour diagram is based on 10 by 10 points then only 3 000 points are considered in the calculation. In contrast, we find that to adequately investigate the structure associated with five simultaneous shape-degrees of freedom almost 3 000 000 grid points, that is, 1000 *times* more points than earlier calculations purporting to be multi-dimensional are required.

The technique we use here to investigate the structure of the multidimensional surface is to employ imaginary water flows^{16,24)} in the calculated 5-dimensional potential-energy surface. For example, we imagine that we stepwise flood, in intervals of 1 MeV, the second minimum with water. During the flooding process we check at what water level a pre-selected “exit” grid point that is clearly in the fission valley near scission gets “wet”. When this happens, then the water level has passed the threshold energy level for fission. We can determine the saddle-point energy to desired accuracy by repeating the filling procedure with successively smaller stepwise increases of the water level. The saddle-point shape can also be obtained from this procedure.

Once the threshold energies for fission have been identified, it is of interest to establish if structure effects in the potential energy provide a mechanism for multi-mode fission, such as the well-known three-peaked mass distribution in ²²⁸Ra fission.⁵⁾ To look for such structures we ask if there are valleys of distinctly different character running in the fission direction of increasing Q_2 . For 10 or more fixed Q_2 values beyond the outer saddle region, we determine all minima in the remaining 4-dimensional space of the two fragment deformations, neck size and mass asymmetry. We find that there are usually two (but sometimes more) distinct valleys in the region beyond the second saddle point, one corresponding to a mass asymmetry α_g of about $[140 - (A - 140)]/A$ and one corresponding to mass symmetry $\alpha_g = 0$. To understand the significance of these valleys it is necessary to study their interconnections in the five-dimensional deformation space.

Variations of the flooding algorithm allow us to determine that separate saddle points provide entries to the two valleys and the respective energies of these saddle points. Once the lowest saddle has been determined we may block the water flow across this saddle by building an imaginary dam across the saddle region. We can also totally block the water flow beyond a selected maximum Q_2 . This prevents water from flowing down one valley and up “the back way” into the other valley. To determine the height of the ridge between the two valleys along their entire length we study for each fixed Q_2 the remaining 4-dimensional space in which the two valleys correspond to two minima and the ridge to the saddle separating them. We use the flooding algorithm in four dimensions to locate this saddle/ridge.

V. Calculated Results

In general our calculated potential-energy surfaces exhibit a complex structure with multiple minima, maxima, saddle points and valleys. Structures significant in fission are extracted by use of the water immersion techniques outlined above. For nuclei in the radium through light actinide region we find consistently that beyond the second minimum the potential-energy surfaces are dominated by two valleys leading to symmetric and asymmetric division into two fragments. The two valleys are separated from the second minimum by *different* saddle points and from each other by a ridge. We find that for ²²⁸Ra the ridge peaks at 2.47 MeV above the entrance saddle to the symmetric valley, whereas

Table 1 Macroscopic model parameters of the FRLDM (1992) and obtained in the present adjustment using barrier heights obtained in our five-dimensional calculation

Constant	FRLDM (1992)	Current fit
a_v	16.00126	16.02444
κ_v	1.92240	1.94149
a_s	21.18466	21.39654
κ_s	2.34500	2.36891
a_0	2.61500	1.08654
c_a	0.10289	0.16197

for ²³²Th it peaks at 1.56 MeV. For ²³⁴U the ridge only rises marginally above the entrance saddle to the symmetric valley. For still heavier systems such as ²⁴⁰Pu we find that the symmetric valley emerges as a “side valley” to the asymmetric valley at some point beyond a single outer saddle at the beginning of the asymmetric valley. Calculated features of the five-dimensional potential-energy surface for ²³²Th are illustrated in **Fig. 4**.

In our calculated potential-energy surfaces we can for each nuclide determine the value of the mass-asymmetry coordinate α_g at the bottom (minimum) of the asymmetric valley. This value is almost independent of Q_2 from slightly beyond the outer saddle to scission; to be specific we use below the mass asymmetry at $Q_2 = 100$ in our comparisons. As discussed above we can directly relate this coordinate to the final heavy and light fragment masses M_H and M_L . In **Fig. 5** we compare heavy and light fragment masses calculated in this way with experimental data. The mean deviation between calculations and experiment is only 3.0 nucleons.

We have also calculated outer barrier heights and compared them to experimental barrier heights for 31 nuclei from ⁷⁰Se to ²⁵²Cf, cf. **Fig. 6**. Because fission saddle points in our five-dimensional deformation spaces are systematically lower than in earlier, lower-dimensional spaces a readjustment of the macroscopic-model constants is necessary to avoid systematic errors in the calculated fission-barrier heights. We here perform such a readjustment in a manner similar to how our FRLDM (1992) constants were determined.¹¹⁾ Only 6 constants are varied; the others remain unchanged. A comparison between the old and the preliminary new constants is found in **Table 1**. In the FRLDM (1992) the mass-model error was 0.779 MeV, and the barrier rms error was 1.40 MeV. We now obtain a mass-model error of 0.759 MeV, and a barrier rms error of 1.08 MeV for a larger and slightly different barrier data set. Because there is a change in barrier deformations for the new set of constants, an iterative procedure is required to determine a final set of FRLDM model parameters (new saddle-point deformations have to be calculated with the new parameters, parameters must be redetermined, and so on). We expect the converged results of such an iteration will not differ by too much from the first iteration presented here.

Finally we give a result from our study of SHE fission-fusion potential-energy surfaces for the compound system ²⁷⁰110. For heavy ions with $A = 208$ and $A = 62$, Q_2 at

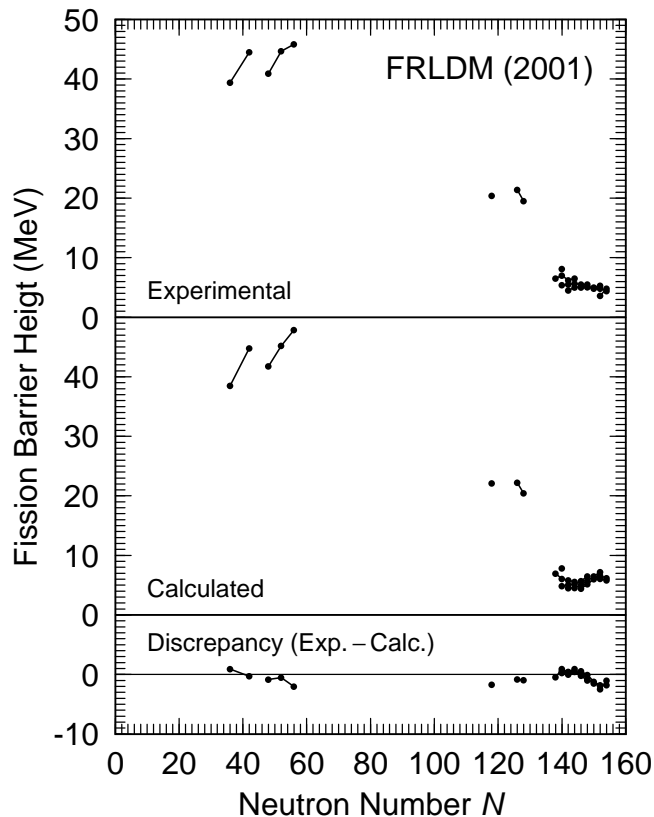


Fig. 6 Comparison of calculated and experimental fission-barrier heights for nuclei throughout the periodic system, after a preliminary readjustment of the macroscopic model constants. It is assumed here that the saddle-point shapes are not affected by the readjustment. Experimental barriers are well reproduced by the calculations, the rms error is only 1.08 MeV for 31 nuclei. In the actinide region it is the outer of the two barriers that are compared.

touching is 40.4 in our units. At our grid point $Q_2 = 42.47$ we find two and only two valleys with mass ratios 162/108 and 200/70 and depths -6.77 MeV and -2.90 MeV, respectively. The ridge between the two valleys is 4.16 MeV high. Clearly a cold-fusion channel exists here, stabilized by a high ridge. However, this valley corresponds to a shape with a fairly large neck diameter. The touching configuration, with no neck, has a much higher energy of 7.72 MeV. Thus this cold-fusion touching configuration is on the side of a hill in five-dimensional space. It slopes down towards two valleys: (1) a “cold-fusion” valley at -2.90 MeV which is separated from a (2) deeper “fission valley” at -6.77 MeV by a more than 4 MeV high ridge.

In summary, with our complete, five-dimensional calculations of potential-energy surfaces, (1) we obtain realistic, multi-mode potential-energy surfaces that correlate closely with the multi-mode fission data seen in experiments, (2) we calculate accurately the average mass asymmetries in asymmetric fission, (3) we obtain observed barrier heights for fission barriers throughout the periodic system, and (4) for superheavy systems we observe a shell-stabilized “cold-fusion” channel that persists to very compact shapes.

References

- 1) O. Hahn and F. Strassmann, *Naturwiss.* **27**, 11 (1939).
- 2) L. Meitner and O. R. Frisch, *Nature* **143**, 239 (1939).
- 3) N. Bohr and J. A. Wheeler, *Phys. Rev.* **56**, 426 (1939).
- 4) S. Frankel and N. Metropolis, *Phys. Rev.* **72**, 914 (1947).
- 5) E. Konecny, H. J. Specht, and J. Weber, *Proc. Third IAEA Symp. on the Physics and Chemistry of Fission*, Rochester, 1973, vol. II (IAEA, Vienna, 1974) p. 3.
- 6) T. Ohtsuki, H. Nakahara, and Y. Nagame, *Phys. Rev. C* **48**, 1667 (1993).
- 7) Y. Nagame, I. Nishinaka, K. Tsukada, S. Ichikawa, H. Ikezoe, Y. L. Zhao, Y. Oura, K. Sueki, H. Nakahara, M. Tanikawa, T. Ohtsuki, K. Takamiya, K. Nakanishi, H. Kudo, Y. Hamajima, and Y. H. Chung, *Radiochimica Acta*, **78**, 3 (1997).
- 8) Y. L. Zhao, I. Nishinaka, Y. Nagame, K. Tsukada, M. Tanikawa, K. Sueki, Y. Oura, S. Ichikawa, H. Ikezoe, T. Ohtsuki, H. Kudo, and H. Nakahara, *J. Alloys and Comp.* **271**, 327 (1998).
- 9) V. M. Strutinsky, *Nucl. Phys.* **A95**, 420 (1967).
- 10) V. M. Strutinsky, *Nucl. Phys.* **A122**, 1 (1968).
- 11) P. Möller, J. R. Nix, W. D. Myers, and W. J. Swiatecki, *Atomic Data Nucl. Data Tables* **59**, 185 (1995).
- 12) P. Möller, J. R. Nix, and W. J. Swiatecki, *Nucl. Phys.* **A492**, 349 (1989).
- 13) P. Möller and J. R. Nix, *Nucl. Phys.* **A281**, 354 (1977).
- 14) J. R. Nix, *Nucl. Phys.* **A130**, 241 (1969).
- 15) B. Hayes, *Am. Sci.* **88**, 481 (2000).
- 16) P. Möller and A. Iwamoto, *Phys. Rev. C* **6104**, 7602 (2000).
- 17) P. Möller, D. G. Madland, A. J. Sierk, and A. Iwamoto, *Tours 2000, Tours Symposium on Nuclear Physics IV*, Tours, France September 4–7, 2000, and AIP Conference Proceedings **561**, p. 455 (2001).
- 18) D. C. Hoffman and M. M. Hoffman, *Ann. Rev. Nucl. Sci.* **24**, 151 (1974).
- 19) L. Dematte, C. Wagemans, R. Barthelemy, P. Dhondt, and A. Deruytter, *Nucl. Phys.* **A617**, 331 (1997).
- 20) K.-H. Schmidt, S. Steinhäuser, C. Böckstiegel, A. Grewe, A. Heinz, A. R. Junghans, J. Benlliure, H.-G. Clerc, M. de Jong, J. Müller, M. Pfüntzer, and B. Voss, *Nucl. Phys.* **A665**, 221 (2000).
- 21) S. Åberg, H. Flocard, and W. Nazarewicz, *Ann. Rev. Nucl. Sci.* **40**, 439 (1990).
- 22) J. L. Egido, L. M. Robledo, and R. R. Chasman, *Phys. Lett.* **B393**, 13 (1997).
- 23) J. F. Berger, M. Girod, and D. Gogny, *Nucl. Phys.* **A502**, c85 (1989).
- 24) A. Mamdouh, J. M. Pearson, M. Rayet, and F. Tondeur, *Nucl. Phys.* **A644**, 389 (1998).